Lattice dynamics properties of chalcopyrite $ZnSnP_2$: Density-functional calculations by using a linear response theory*

You Yu(虞游)[1,†], Yu-Jing Dong(董玉静)[2], Yan-Hong Shen(沈艳红)[1], Guo-Dong Zhao(赵国栋)[1], Xiao-Lin Zheng(郑小林)[1], and Jia-Nan Sheng(盛佳南)[1]

[1] *College of Optoelectronic Technology, Chengdu University of Information Technology, Chengdu* 610225, *China*
[2] *School of Science and Technology, Xinyang University, Xinyang* 464000, *China*

(Received 10 December 2016; revised manuscript received 20 January 2017; published online 20 February 2017)

We present a first-principles study of the structural, dielectric, and lattice dynamical properties for chalcopyrite semiconductor $ZnSnP_2$. The structural properties are calculated using a plane-wave pseudopotential method of density-functional theory. A linear response theory is used to derive Born effective charge tensors for each atom, dielectric constants in low and high frequency limits, and phonon frequencies. We calculate all zone-center phonon modes, identify Raman and infrared active modes, and report LO–TO splitting of the infrared modes. The results show an excellent agreement with experiment and propose several predictive behaviors.

Keywords: phonon, Born effective charge, dielectric permittivity, linear response theory

PACS: 63.20.dk, 63.20.–e, 63.20.D– **DOI:** 10.1088/1674-1056/26/4/046302

1. Introduction

Ternary ABC_2 semiconducting crystals having chalcopyrite structure have been synthesized from I–III–VI_2 and II–IV–V_2 elements. They are derived from their binary analog zinc-blende II–VI and III–V semiconductors, respectively. $ZnSnP_2$ is a relatively little studied ternary chalcopyrite semiconductor material of the II–IV–V_2 family. Recently, $ZnSnP_2$ has received a great deal of attention as a photovoltaic material.[1] It is a promising candidate, given that its direct band gap of 1.68 eV[2] yields a high theoretical photovoltaic conversion efficiency close to 30% in AM1.5G sunlight at the Shockley–Queisser limit.[3] Undoped $ZnSnP_2$ typically shows p-type conductivity.[4,5]

Born effective charges, low frequency dielectric constants, and the phonon frequencies provide important information about the properties of the materials. The vibrational properties of $ZnSnP_2$ have been widely investigated for the past 40 years by a number of experimental and theoretical methods.[6–10] Experimentally, the infrared (IR) reflectivity of $ZnSnP_2$ (at 295 K) was measured by Zlatkin *et al.*[6] in 1969, and the corresponding optical constants and vibrational frequencies are determined. However, no Raman-active modes are given. Employing Raman (R) spectroscopy and an infrared spectrometer, Mintairov *et al.*[7] measured the Raman scattering and infrared reflectivity, respectively. Both Raman-active and infrared-active modes are reported in Ref. [7]. Nevertheless, some modes have not been found in previous experiments.

Several earlier calculations have been performed to study the dynamical properties of $ZnSnP_2$ by using phenomenological models, such as rigid ion and Keating's models. The phonon dispersion relations over the entire Brillouin zone of $ZnSnP_2$ were calculated using the rigid ion model by Mintairov *et al.*[7] The zone-centered phonons of $ZnSnP_2$ have been studied using Keating's models by Bettini.[10] In addition, the phonon frequencies values have been calculated by transfer of the spectral pattern.[9] The theoretical research mentioned above has a limitation, that is to say, the potentials in the calculations depend on experimental value. Identification of vibration modes in experimental measurements is sometimes incomplete, partly because of the complexity of the dispersion scheme in the chalcopyrite structure and partly because of experimental errors.

Nowadays the first-principles calculation has proved to be a powerful tool for the study of lattice dynamical properties. First-principles calculations of dynamical properties of $ZnSnP_2$ have been studied by Lazewski *et al.*[8] The calculations were done by the direct method[11,12] from HF forces arising when a single atom is displaced from its equilibrium position. Generally, the first-principles investigation of phonon frequencies is mainly divided into two categories: the direct method and the linear-response method.[13,14] The longitudinal–optical/transverse–optical (LO–TO) splitting of

*Project supported by the Open Research Fund of Computational Physics Key Laboratory of Sichuan Province, Yibin University (Grant No. JSWL2014KFZ01), the Scientific Research Fund of Sichuan Provincial Education Department, China (Grant No. 16ZB0209), the Scientific Research Foundation of Chengdu University of Information Technology, China (Grant No. J201611), and the National Natural Science Foundation of China (Grant No. 11547224).

†Corresponding author. E-mail: yy2012@cuit.edu.cn

© 2017 Chinese Physical Society and IOP Publishing Ltd

the infrared active modes based on effective charges and dielectric tensors are not directly given for the direct method. However, the two quantities can be calculated directly by a linear response method based on density functional perturbation theory (DFPT).[15,16] Although there are some studies of lattice dynamical properties for $ZnSnP_2$, they are still an important part of a full understanding of the phonon in the material.

In this paper we present first-principles linear response theory to investigate the lattice dynamics properties, such as Born effective charge tensors for each atom, dielectric constants in low and high frequency limits, and phonon frequencies. This paper is organized as follows. In Section 2, we briefly review the underlying theoretical methods. In the following sections, results are presented and discussed for geometry parameters (Subsection 3.1), Born effective charge tensor (Subsection 3.2), phonon frequencies (Subsection 3.3), and dielectric tensor (Subsection 3.4), respectively. Finally, conclusions are given in Section 4.

2. Computational method

Our calculations were performed with the ABINIT package,[17] which is based on density-functional theory (DFT) using the pseudopotential method and a plane-wave expansion of the wave functions. The interactions between the ions and valence electrons were described using norm-conserving local density approximation (LDA) pseudopotentials which are generated in the scheme of Troullier–Martins (TM).[18–21] For the exchange–correlation potential we have used the local density approximation data of Ceperly–Alder, as parametrized by Perdew and Wang.[22] The Zn ($3d^{10}$, $4s^2$), Sn ($5s^2$, $5p^2$), and P ($3s^2$, $3p^3$) orbitals are treated as valence states. The pseudopotentials used in the present calculations are soft potentials of the TM type, available on the ABINIT website. The density-functional perturbation theory is the basis of the linear-respond approach. Phonon frequencies and atoms displacements are obtained using the linear-respond method, which avoids the use of supercells and allows the calculation of dynamical matrix at arbitrary $\boldsymbol{q}$ vectors. Technical details on the computation of responses to atoms displacements can be found in Refs. [23] and [24], while reference [14] presents the subsequent computation of phonon frequencies, Born effective charge tensors for each atom, and dielectric constants.

The calculations were carried out with a 36-hartree plane-wave energy cutoff, and the tetragonal Brillouin zone (BZ) was sampled with a regular and shifted $4\times4\times4$ k-point mesh. Convergence tests show that the BZ sampling and the kinetic energy cutoff are sufficient to insure an excellent convergence within 1 cm^{-1} for the calculated phonon frequencies.

3. Results and discussion

3.1. Structural optimization

The body-centered tetragonal chalcopyrite structure of $ZnSnP_2$ is shown in Fig. 1. Each unit cell contains four formula units and the point group is $\bar{4}2m\,(D_{2d})$. The chalcopyrite structure is deduced from that of the zinc-blende by the replacement of the cationic sublattice by two different atomic species. In general, II–V and IV–V bond lengths, denoted by $d_{\mathrm{II-V}}$ and $d_{\mathrm{IV-V}}$, respectively, are not equal, which is mentioned in the substitution results in two different structural deformations: the first one is the relocation of anions in the x–y plane which is characterized by parameter $u = 0.25 + \left(d^2_{\mathrm{II-V}} - d^2_{\mathrm{IV-V}}\right)/a^2$. Here, a is the lattice constant in the x or y direction. The second consequence of differing anion-cation bond lengths is a deformation of the unit cell along the z direction to a length c, which is generally different from $2a$. This tetragonal distortion is characterized by the quantity c/a. For real compounds of pnictide II–IV–V_2 groups in most cases $c/a = 1.769$–2.016 and $u = 0.214$–0.304.[25] The unit vectors of the primitive cell are (a, 0, 0), (0, a, 0), ($a/2$, $a/2$, $c/2$). The cations are located at $4a$ and $4b$ while anions are located at $8d$ Wyckoff positions. Ion positions can be generated using the following minimum set of (x, y, z) coordinates expressed in units of the a and c constants.

Group II: (0, 0, 0), (0, 1/2, 1/4);

Group IV: (0, 0, 1/2), (0, 1/2, 3/4);

Group V: (u, 1/4, 1/8), ($-u$, 3/4, 1/8), (3/4, u, 7/8), (1/4, $-u$, 7/8).

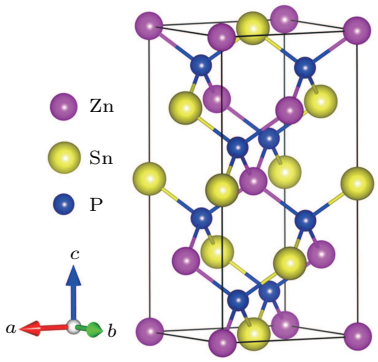


Fig. 1. (color online) Crystal structure of $ZnSnP_2$ (chalcopyrite-type; body-centered tetragonal-$I\bar{4}2d$).

The ground state structural properties are obtained by minimization of the total energy with respect to the unit cell volume. The structural parameters are obtained by optimizing lattice constants and atomic coordinates until all force components are below 5×10^{-5} hartree/Bohr (1 hartree = 27.2114 eV). Table 1 summarizes our results obtained after relaxation of the lattice constants, as well as the available calculated[8,26,27] and experimental values.[5,28] For $ZnSnP_2$, optimization of unit cell geometry within LDA leads to $a = 5.622$ Å, $c = 11.233$ Å. The calculated lattice constants are underestimated with the maximal error of 0.7%, which is

typically the expected precision for the LDA. Even comparison with experimental values at the lowest temperatures available is, strictly speaking, not correct, since it neglects the anharmonic effect of the zero-point vibrations. Even so, the calculated lattice parameters are found to be in good agreement with the experimental ones. The optimized results show our calculation method is feasible and we will adopt the optimized structure parameters to calculate other properties.

Table 1. The equilibrium lattice constant a (c) (in unit Å), axial ratio c/a and internal parameter for $ZnSnP_2$.

Method	a	c	c/a	u
ABINIT-LDA (Present work)	5.622	11.233	1.998	0.231
VASP-LDA (Ref. [8])	5.606	11.089	1.978	0.227
VASP-GGA+U (Ref. [26])	5.706	11.443	2.005	0.228
VASP-HSE06 (Ref. [26])	5.671	11.352	2.002	0.232
CASTEP-LDA (Ref. [27])	5.638	11.228	1.991	0.25
Exp. (Ref. [5])	5.651	11.302	2.000	0.239
Exp. (Ref. [28])	5.652	11.305	2.000	0.229

3.2. Born effective charge tensors

The Born effective charge tensor quantifies the macroscopic electric response of a crystal to the internal displacements of its atoms. They are important quantities in obtaining the LO–TO phonon splitting, also they provide some information about the ionicity of the material. For atom κ, the Born effective charge tensor $Z^*_{\kappa,\beta\alpha}$ is defined as the proportionality coefficient relating, at linear order, the polarization per unit cell, created along the direction β, and the displacement along the direction α of the atoms belonging to the sublattice κ, under the condition of a zero electric field.[14] In this work, the Born effective charge tensors $Z^*_{\kappa,\beta\alpha}$ for each atom of $ZnSnP_2$ are calculated by DFPT.

Values of the calculated Born effective charge of $ZnSnP_2$ are presented in Table 2. To the best of our knowledge, no other first-principles calculations of the Born effective charge for $ZnSnP_2$ exist. The form of $Z^*_{\kappa,\beta\alpha}$ for atom κ depends on the site symmetry of the ions. The point symmetries at the site of Zn ion and Sn ion are S_4 ($4a$ sites) and S_4 ($4b$ sites), respectively. For P ion, the point symmetry at the site is C_2 ($8d$ sites). The effective charge tensors for cations are diagonal and obey $Z^*_{xx} = Z^*_{yy} \neq Z^*_{zz}$, as required by symmetry for a tetragonal crystal. According to the calculation results, cations have diagonal Born effective charges with $Z^*_{\mathrm{Zn},xx} = Z^*_{\mathrm{Zn},yy} = 1.76$, $Z^*_{\mathrm{Zn},zz} = 1.73$, and $Z^*_{\mathrm{Sn},xx} = Z^*_{\mathrm{Sn},yy} = 2.50$, $Z^*_{\mathrm{Sn},zz} = 2.64$. Z^* of cations are almost diagonal with an anisotropy of 2% for Zn and 5% for Sn, respectively. The effective charge tensors have nearly spherical symmetry, with small tetragonal distortion caused by $c/2a \neq 1$. P ions, located at lower symmetry sites, have nondiagonal and anisotropic Z^*. For all anions, $Z^*_{\mathrm{P},zz} = -2.18$ while $Z^*_{\mathrm{P},xx}$ and $Z^*_{\mathrm{P},yy}$ take the value -1.99 or -2.27 depending on the distortion of u. Also, depending on the u distortion being along the x or y direction, the nondiagonal components $Z^*_{\mathrm{P},zx} = \pm 0.02$, $Z^*_{\mathrm{P},xz} = \pm 0.13$ or $Z^*_{\mathrm{P},yz} = \pm 0.13$, $Z^*_{As,zy} = \pm 0.02$ are different than zero. We can see that the shape of Z^* for P ions is far from a sphere. This behavior has also been observed in the case of other chalcopyrite semiconductors.[29–32]

The average eigenvalues for cations and anions are comparable to the values in Ref. [10]. The calculated average eigenvalues ($Z^*(\bar{\lambda})$) in our work for Zn, Sn, and P are 1.75, 2.55, and -2.15, respectively. Obviously, the three atoms have smaller effective charges than their formal charges, $+2$, $+4$, and -3 for Zn, Sn, and P, respectively. Such difference can be derived from the strong covalent characteristic for bonds. To the best of our knowledge, no other first-principle calculations and experimental data of Z^* for $ZnSnP_2$ exist. We have compared our results with other literature data calculated with a different force-field model.[10] This discrepancy is pronounced for the effective charges in Ref. [10] obtained by a least square fit of the phonon energies and Coulomb splittings, probably because of the use of approximate eigenvectors and assumptions about the dynamical charges. Earlier results by Akdogan *et al.*[31] gave Born effective charges of $CuGaS_2$ with the same linear response as ours, and average of eigenvalues $Z^*(\bar{\lambda})$ displayed a good agreement with experimental data.

Table 2. Calculated Born effective charge tensors, Z^*, eigenvalues of the symmetric part of $Z^*(\lambda)$, average of eigenvalues $Z^*(\bar{\lambda})$, and force-field model effective charges of Ref. [10].

Atom	Z^*	$Z^*(\lambda)$	$Z^*(\bar{\lambda})$	Point charge of Ref. [10]
Z^*_{Zn}	$\begin{pmatrix} 1.76 & 0.13 & 0.00 \\ -0.13 & 1.76 & 0.00 \\ 0.00 & 0.00 & 1.73 \end{pmatrix}$	$\begin{bmatrix} 1.76 \\ 1.76 \\ 1.73 \end{bmatrix}$	1.75	0.9
Z^*_{Sn}	$\begin{pmatrix} 2.50 & -0.31 & 0.00 \\ 0.31 & 2.50 & 0.00 \\ 0.00 & 0.00 & 2.64 \end{pmatrix}$	$\begin{bmatrix} 2.64 \\ 2.50 \\ 2.50 \end{bmatrix}$	2.55	0.4
$Z^*_{\mathrm{P_1}}$	$\begin{pmatrix} -1.99 & 0.00 & 0.00 \\ 0.00 & -2.27 & 0.13 \\ 0.00 & 0.02 & -2.18 \end{pmatrix}$	$\begin{bmatrix} -2.29 \\ -2.16 \\ -1.99 \end{bmatrix}$	–2.15	–0.65
$Z^*_{\mathrm{P_2}}$	$\begin{pmatrix} -2.27 & 0.00 & 0.13 \\ 0.00 & -1.99 & 0.00 \\ 0.02 & 0.00 & -2.18 \end{pmatrix}$	$\begin{bmatrix} -2.29 \\ -2.16 \\ -1.99 \end{bmatrix}$	–2.15	–0.65

3.3. Phonons

The crystal symmetry of $ZnSnP_2$ is body-centered tetragonal with a centro-symmetric space group $I\bar{4}2d$ and a corresponding $\bar{4}2m$ point group. Positions of nonequivalent atoms are indicated in Fig. 2. There are four distinct P, two Zn, and two Si atoms. Transformation properties of these atoms under symmetry operations of the space group are noted in Table 3. As a tetragonal crystal, $ZnSnP_2$ has phonon dispersion relations consisting of 24 branches whose group theoretical analysis at the BZ center (Γ) yields a decomposition into

$$\Gamma = 1A_1 + 2A_2 + 3B_1 + 4B_2 + 7E, \quad (1)$$

where E is a double degenerate mode. The acoustic modes correspond to one B_2 and one E mode. For optical modes, the irreducible representation is

$$\Gamma_{\text{opt}} = 1A_1 + 2A_2 + 3B_1 + 3B_2 + 6E. \quad (2)$$

The A_1 and B_1 modes are Raman-active, B_2 and E modes are both Raman- and IR-active, and the A_2 mode is silent. These IR modes are polar modes and subject to an LO–TO splitting. Symmetry coordinates for the onefold A and B representations are given in Figs. 2 and 3, respectively, and for the twofold E representations in Fig. 4. A detailed discussion can be found in Ref. [33].

Table 3. Character table for the D_{2d} point group (tetragonal).

D_{2d} ($\bar{4}2m$)	E	$2S_4$	C_2	$2C_2'$	$2\sigma_d$	Symmetry	Activity	Number	
								Optical	Acoustic
A_1	1	1	1	1	1	x^2+y^2, z^2	R	1	0
A_2	1	1	1	–1	–1	–	silent	2	0
B_1	1	–1	1	1	–1	x^2-y^2	R	3	0
B_2	1	–1	1	–1	1	xy	R, IR	3	1
E	2	0	–2	0	0	$(x, y), (xz, yz)$	R, IR	6	1

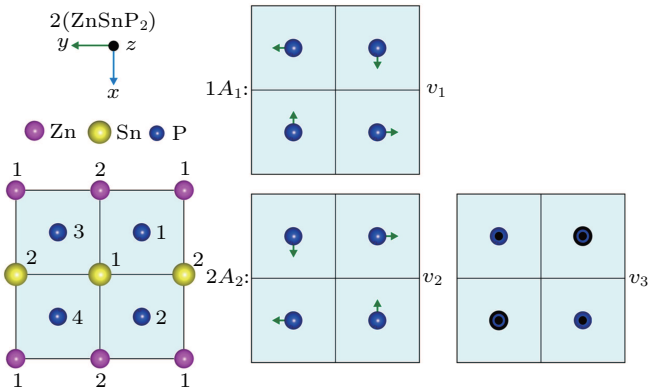


Fig. 2. (color online) (001) projection of unit cell showing positions of four nonequivalent P atoms, the two nonequivalent Zn atoms and the two nonequivalent Sn atoms. Symmetry coordinates for A modes ($1A_1 + 2A_2$); displacements in the xy plane are represented by arrows and displacements in the z direction by open and closed circles.

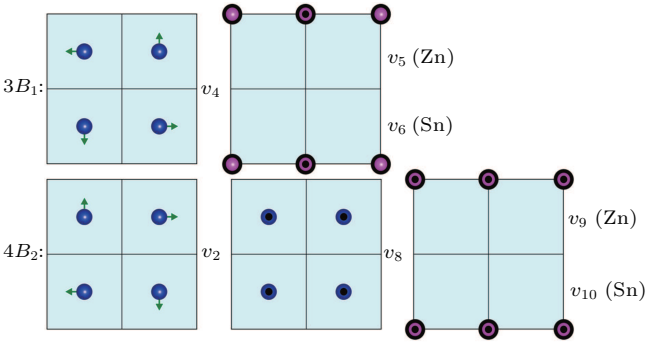


Fig. 3. (color online) Symmetry coordinates for B modes ($3B_1 + 4B_2$); displacements in the xy plane are represented by arrows and displacements in the z direction by open and closed circles.

Complete phonon branches of $ZnSnP_2$ are plotted for the high-symmetry lines in the BZ together with the corresponding phonon density of states (DOS) in Fig. 5. An interesting feature of acoustic branches around the Γ point is observed, especially along Γ–X and Γ–Z directions. In order to obtain the phonon dispersion curves throughout the BZ, the dynamical matrices are obtained 4×4×4 grid of q points, and real space force constants are then found by Fourier transform of the dynamical matrices. The acoustic sum rule is applied to force the three acoustic phonon frequencies at the Γ point equal to zero strictly as being implied by translation symmetry.

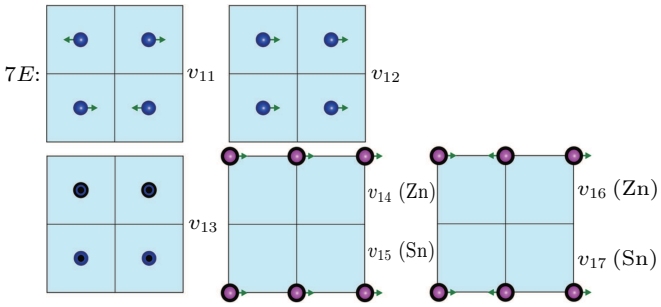


Fig. 4. (color online) Symmetry coordinates for E modes ($7E$); displacements in the xy plane are represented by arrows and displacements in the z direction by open and closed circles.

In Table 4, we compare calculated phonon frequencies of $ZnSnP_2$ at the Γ point with the measured Raman[7] and infrared[6,7] values. For comparison, we cite also the phonon frequencies from theoretical calculations through direct methods[8] and a classical model.[7,9,10] As shown in Fig. 5 and Table 4, three groups of modes can be identified. A clear gap exists between the twelve upper energy branches and the remaining twelve branches. The low frequency group of modes has a range of values from 82 cm^{-1} to 115 cm^{-1} and the medium frequency group of modes has a range of values from 180 cm^{-1} to 207 cm^{-1}. The highest frequency group of modes can be up to 370 cm^{-1}. Unfortunately, some vibration modes have not been observed in previous experiments, including infrared and Raman measurements. To get more accurate measurements, inelastic neutron scattering experiments should be adopted, but it is not available in previous works. Otherwise, for some of the modes there are large differences among the reported theoretical frequencies, for example the highest frequency B_2 mode ranges from 350 cm^{-1} to 375 cm^{-1}. Our calculation shows that the mode is at 365 cm^{-1}, which is in very good agreement with experiments.[6,7] It makes us very confident in the prediction of the frequencies for the others.

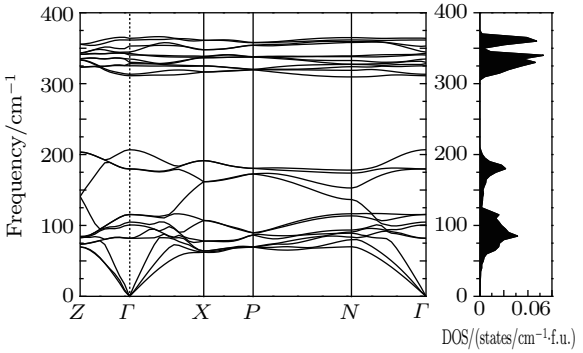


Fig. 5. Calculated phonon dispersion curves along symmetry lines in the Brillouin zone and the corresponding phonon density of states (DOS) for $ZnSnP_2$.

It should be noted that the direct method was performed to calculate the phonon frequencies of $ZnSnP_2$ by Lazewski *et al.*[8] Although the calculated frequencies show a better agreement with ours, the LO–TO splittings are not discussed. This is because the splitting depends on the effective charges and dielectric tensors of the system, which are not directly accessible to the direct method. The IR modes group into modes with displacements either in the x, y plane or along the z direction. The E mode has a displacement pattern in the x, y plane, and the B_2 mode has displacements along the z direction. The LO–TO splittings for B_2 and E modes are presented in Table 4 and the values of LO–TO splitting agree well the experimental results.[6,7] The missing modes in the experiment are predicted successfully. For $ZnSnP_2$, the LO–TO splitting is small, ranging from 0 cm^{-1} to 10 cm^{-1}. The splitting is even zero in the low frequency region, because the low frequency modes are essentially the folded acoustic modes, they correspond to whole molecular units moving relative to each other. The largest difference appears on the E mode with the highest frequency. The large LO–TO splittings of these modes suggest they involve large effective charges and make large contributions to the static dielectric tensor of $ZnSnP_2$. A similar splitting case occurs for $CuGaSe_2$ and the results can be found in Ref. [29].

Table 4. A comparison of calculated phonon frequencies (in unit cm^{-1}) at the Γ point with Raman and infrared data as well as with other theory values. Two numbers in a row correspond to LO/TO frequencies.

Mode		Theory/present	Experiment			Theory			
			IR[6]	IR[7]	R[7]	*Ab initio*[8]	Estimated[9]	Keating's model[10]	Rigid ion model[7]
A_1	R	313			309	298	309	304	307
A_2	silent	311			295	308			292
	silent	345			333	332			331
B_1	R	105				106	106	138	124
	R	207				205	191	214	208
	R	362			353	358	333	346	352
B_2	R, IR	101/100				105/101	98	149/148	140/139
	R, IR	330/328	–/327		347/–	353/321	331	345/335	329/324
	R, IR	365/364	–/368		365/–	360/359	350	375/354	372/348
E	R, IR	82/82				77/77	85	125/125	115/115
	R, IR	115/115				119/116	108	165/164	154/153
	R, IR	180/180				182/179	157	188/187	190/189
	R, IR	328/325		318/313	317/–	325/321	318	312/311	317/315
	R, IR	340/335	–/327	339/328	328/–	331/327	321	329/328	334/333
	R, IR	353/343	–/368	360/342	342/–	354/331	337	375/345	378/350

3.4. Lattice dielectric properties

The dielectric tensor for a tetragonal system such as this will be diagonal with two distinct elements. For $ZnSnP_2$, the calculated electronic (ε_∞) and static (ε_0) dielectric tensors are diagonal and have two independent components $\varepsilon^{\perp}$ and $\varepsilon^{||}$ perpendicular to and along the c axis, respectively. In Table 5 we compare the values calculated for the dielectric tensor of $ZnSnP_2$ with theoretical and experimental data available. The electronic dielectric constants are calculated to be $\varepsilon_\infty^{\perp} = \varepsilon_\infty^{xx} = \varepsilon_\infty^{yy} = 11.91$ and $\varepsilon_\infty^{||} = \varepsilon_\infty^{zz} = 12.01$. The static dielectric tensor can be decomposed into contributions of different modes and calculated by the generalized Lyddane–Sachs–Teller (LST) relation:[34]

$$\varepsilon_0 = \varepsilon_\infty \prod_m \frac{\omega_{\mathrm{LO},m}^2}{\omega_{\mathrm{TO},m}^2}, \tag{3}$$

where the frequencies $\omega_{\mathrm{LO},m}$ and $\omega_{\mathrm{TO},m}$ are the long wavelength limits for longitudinal and transverse vibrations, respectively. According to the LST relation, the static dielectric constants of ε_0 both directions are $\varepsilon_0^{\perp} = \varepsilon_0^{xx} = \varepsilon_0^{yy} = 13.74$ and $\varepsilon_0^{||} = \varepsilon_0^{zz} = 13.86$, respectively, showing a nearly isotropic character. The averages of ε_∞ and ε_0, obtained from the expression ε_∞ (or ε_0) = $(2\varepsilon_\infty^{\perp} + \varepsilon_\infty^{||})/3$ are also shown in Table 5. The components of ε_0 are much larger than those of ε_∞ as a consequence of the significant contribution to the low-

frequency dielectric permittivity tensor due to ionic displacements.

Table 5. Static and high frequency dielectric tensor components of $ZnSnP_2$.

	$\varepsilon_\infty^{\parallel}$	$\varepsilon_\infty^{\perp}$	ε_∞	$\varepsilon_0^{\parallel}$	$\varepsilon_0^{\perp}$	ε_0
This work	12.01	11.91	11.94	13.86	13.74	13.78
Exp. (Ref. [6])			8.1±0.2			10.0±0.4
Calc. (Ref. [35])						9.90
Calc. (Ref. [36])				12.68	12.75	12.73
Calc. (Ref. [27])						10.08

The dielectric properties of $ZnSnP_2$ have not been studied very much experimentally. We are only aware of the measurement of the dielectric constant of $ZnSnP_2$ in which a value of $\varepsilon_\infty \approx 8.1$ (or $\varepsilon_0 \approx 10.0$) has been reported in Ref. [6]. On the theoretical side, the dielectric constant has been calculated by Verma *et al.*[34] using a plasma oscillations theory. ε_0 from Ref. [35] is 9.90 and seems to be more consistent with the experimental value 10.0. Our calculated values and previous theoretical values[27,36] are calculated by using the DFT and larger than the experimental results. The overestimation of the calculation is a well-known fact of the DFT due to the underestimation of the band gap.[34,37,38] We note that a smaller energy gap E_g yields a larger ε_0 value. This can be explained on the basis of the Penn model.[39] The Penn model is based on the expression $\varepsilon_0 \approx 1 + \left(\hbar\omega_P/E_g\right)^2$. It is clear that ε_0 is inversely proportional to E_g. The dielectric constants calculated in our work deviate from other theoretical data[27,35] because a small band gap was adopted in the calculation.

4. Conclusions

To summarize, we have presented first-principles calculations of the structural, dielectric, and, in particular, of the lattice dynamical properties of the chalcopyrite semiconductor $ZnSnP_2$within the density-functional theory and pseudopotential methods. The optimal ground state structure is studied within the LDA approaches. The relaxed lattice constants are found to be in good agreement with the experimental ones with the maximal error of 0.7%. Born effective charge and dielectric constants are calculated within the linear response theory. The calculated average eigenvalues $Z^*(\bar{\lambda})$ for Zn, Sn, and P are 1.75, 2.55, and −2.15, respectively. They are smaller than their formal charges because of the strong covalent characteristic for bonds. Our theoretical values of dielectric constants tend to be overestimated in LDA calculations due to the underestimation of the band gap. The phonon frequencies at the Γ point of the BZ are calculated and their assignments are given. The LO–TO splittings for B_2 and E modes are presented and the values of LO–TO splitting agree well the infrared and Raman measurements. We believe that our theoretical predictions should be highly valuable for the experimental community in the framework of the characterization of $ZnSnP_2$.

References

[1] Folmer J C W, Tuttle J R, Tu J A and Parkinson B A 1985 *J. Electrochem. Soc.* **132** 1608
[2] St-Jean P, Seryogin G A and Francoeur S 2010 *Appl. Phys. Lett.* **96** 231913
[3] Shockley W and Queisser H J 1961 *J. Appl. Phys.* **32** 510
[4] Rubenstein M and Ure R W 1968 *J. Phys. Chem. Solids* **29** 551
[5] Vaipolin A A, Goryunova N A, Kleshchinskii L I, Loshakova G V and Osmanov E O 1968 *Phys. Status Solidi B* **29** 435
[6] Zlatkin L B, Markov Yu F, Stekhanov A I and Shur M S 1969 *Phys. Stat. Solidi* **32** 473
[7] Mintairov A M, Sadchikov N A, Sauncy T and Holtz M 1999 *Phys. Rev. B* **59** 15197
[8] Lazewski J and Parlinski K 2001 *J. Alloys Compd.* **328** 162
[9] Ohrendorf F W and Haeuseler H 1999 *Cryst. Res. Technol.* **34** 339
[10] Bettini M 1975 *Phys. Stat. Solidi* **69** 201
[11] Parlinski K, Li Z Q and Kawazoe Y 1997 *Phys. Rev. Lett.* **78** 4063
[12] Kunc K and Martin R M 1982 *Phys. Rev. Lett.* **48** 406
[13] Giannozzi P, Gironcoli S de, Pavone P and Baroni S 1991 *Phys. Rev. B* **43** 7231
[14] Gonze X and Lee C 1997 *Phys. Rev. B* **55** 10355
[15] Baroni S, Giannozzi P and Testa A 1987 *Phys. Rev. Lett.* **58** 1861
[16] Baroni S, Gironcoli S de, Dal Corso A and Giannozzi P 2001 *Rev. Mod. Phys.* **73** 515
[17] Gonze X, Beuken J M, Caracas R, Detraux F, Fuchs M, Rignanese G -M, Sindic L, Verstraete M, Zerah G, Jollet F, Torrent M, Roy A, Mikami M, Ghosez Ph, Raty J Y and Allan D C 2002 *Comput. Mater. Sci.* **25** 478
[18] Goedecker S 1997 *SIAM J. Sci. Comput.* **18** 1605
[19] Payne M C, Teter M P, Allan D C, Arias T A and Joannopoulos J D 1992 *Rev. Mod. Phys.* **64** 1045
[20] Gonze X 1996 *Phys. Rev. B* **54** 4383
[21] Fuchs M, and Scheffler M 1999 *Comput. Phys. Commun.* **119** 67
[22] Perdew J P and Wang Y 1992 *Phys. Rev. B* **45** 13244
[23] Gonze X 1997 *Phys. Rev. B* **55** 10337
[24] Hamann D R, Wu X, Rabe K M and Vanderbilt D 2005 *Phys. Rev. B* **71** 035117
[25] Jaffe J E and Zunger A 1984 *Phys. Rev. B* **29** 1882
[26] Hinuma Y, Oba F, Nose Y and Tanaka I 2013 *J. Appl. Phys.* **114** 043718
[27] Sahin S, Ciftci Y O, Colakoglu K and Korozlu N 2012 *J. Alloys Compd.* **529** 1
[28] Shaposhnikov V L, Krivosheeva A V and Borisenko V E 2012 *Phys. Rev. B* **85** 205201
[29] Parlak C and Eryigit R 2006 *Phys. Rev. B* **73** 245217
[30] Lazewski J, Jochym P T and Parlinski K 2002 *J. Chem. Phys.* **117** 2726
[31] Akdogan M and Eryigit R 2002 *J. Phys.: Condens. Matter* **14** 7493
[32] Yu Y, Zhao B J, Zhu S F, Gao T and Hou H J 2011 *Solid State Sci.* **13** 422
[33] Kaminow I P, Buehler E and Wernick J H 1970 *Phys. Rev. B* **2** 960
[34] Martin R M and Ortiz G 1997 *Phys. Rev. B* **56** 1124
[35] Verma A S and Bhardwaj S R 2006 *Phys. Stat. Solidi* **243** 2858
[36] Chiker F, Abbar B, Bresson S, Khelifa B, Mathieu C and Tadjer A 2004 *J. Solid State Chem.* **177** 3859
[37] Gonze X, Ghosez Ph and Godby R W 1995 *Phys. Rev. Lett.* **74** 4035
[38] Ghosez Ph, Michenaud J P and Gonze X 1998 *Phys. Rev. B* **58** 6224
[39] Penn D R 1962 *Phys. Rev.* **128** 2093